1-1-2007

Search for Stop Production in R-Parity-Violating Supersymmetry at HERA

S. Chekanov
Argonne National Laboratory

M. Derrick
Argonne National Laboratory

S. Magill
Argonne National Laboratory

S. Miglioranzi
Argonne National Laboratory

B. Musgrave
Argonne National Laboratory

See next page for additional authors

Eur. Phys. J. C 50, 269–281 (2007)
DOI 10.1140/epjc/s10052-007-0240-8

THE EUROPEAN PHYSICAL JOURNAL C

Regular Article – Experimental Physics

Search for stop production in R-parity-violating supersymmetry at HERA

The ZEUS Collaboration

S. Chekanov[1,a], M. Derrick[1], S. Magill[1], S. Miglioranzi[1,53], B. Musgrave[1], D. Nicholass[1,53], J. Repond[1], R. Yoshida[1], M.C.K. Mattingly[2], N. Pavel[3,b], A.G.Y. Molina[3], S. Antonelli[4], P. Antonioli[4], G. Bari[4], M. Basile[4], L. Bellagamba[4], M. Bindi[4], D. Boscherini[4], A. Bruni[4], G. Bruni[4], L. Cifarelli[4], F. Cindolo[4], A. Contin[4], M. Corradi[4,54,c], S. De Pasquale[4], G. Iacobucci[4], A. Margotti[4], R. Nania[4], A. Polini[4], L. Rinaldi[4], G. Sartorelli[4], A. Zichichi[4], G. Aghuzumtsyan[5,d], D. Bartsch[5], I. Brock[5], S. Goers[5], H. Hartmann[5], E. Hilger[5], H.-P. Jakob[5], M. Jüngst[5], O.M. Kind[5], E. Paul[5,e], J. Rautenberg[5,55], R. Renner[5], U. Samson[5,f], V. Schönberg[5], M. Wang[5], M. Wlasenko[5], N.H. Brook[6], G.P. Heath[6], J.D. Morris[6], T. Namsoo[6], M. Capua[7], S. Fazio[7], A. Mastroberardino[7], M. Schioppa[7], G. Susinno[7], E. Tassi[7], J.Y. Kim[8,g], K.J. Ma[8,h], Z.A. Ibrahim[9], B. Kamaluddin[9], W.A.T.W. Abdullah[9], Y. Ning[10], Z. Ren[10], F. Sciulli[10], J. Chwastowski[11], A. Eskreys[11], J. Figiel[11], A. Galas[11], M. Gil[11], K. Olkiewicz[11], P. Stopa[11], L. Zawiejski[11], L. Adamczyk[12], T. Bołd[12], I. Grabowska-Bołd[12], D. Kisielewska[12], J. Łukasik[12], M. Przybycień[12], L. Suszycki[12], A. Kotański[13,i], W. Słomiński[13], V. Adler[14], U. Behrens[14], I. Bloch[14], A. Bonato[14], K. Borras[14], N. Coppola[14], J. Fourletova[14], A. Geiser[14], D. Gladkov[14], P. Göttlicher[14,56], I. Gregor[14], T. Haas[14], W. Hain[14], C. Horn[14], B. Kahle[14], U. Kötz[14], H. Kowalski[14], E. Lobodzinska[14], B. Löhr[14], R. Mankel[14], I.-A. Melzer-Pellmann[14], A. Montanari[14], D. Notz[14], A.E. Nuncio-Quiroz[14], R. Santamarta[14], U. Schneekloth[14], A. Spiridonov[14,57], H. Stadie[14], U. Stösslein[14], D. Szuba[14,58], J. Szuba[14,j], T. Theedt[14], G. Wolf[14], K. Wrona[14], C. Youngman[14], W. Zeuner[14], S. Schlenstedt[15], G. Barbagli[16], E. Gallo[16,k], P.G. Pelfer[16], A. Bamberger[17], D. Dobur[17], F. Karstens[17], N.N. Vlasov[17,l], P.J. Bussey[18], A.T. Doyle[18], W. Dunne[18], J. Ferrando[18], D.H. Saxon[18], I.O. Skillicorn[18], I. Gialas[19,66], T. Gosau[20], U. Holm[20], R. Klanner[20], E. Lohrmann[20], H. Salehi[20], P. Schleper[20], T. Schörner-Sadenius[20], J. Sztuk[20], K. Wichmann[20], K. Wick[20], C. Foudas[21], C. Fry[21], K.R. Long[21], A.D. Tapper[21], M. Kataoka[22,59], T. Matsumoto[22], K. Nagano[22], K. Tokushuku[22,60], S. Yamada[22], Y. Yamazaki[22], A.N. Barakbaev[23], E.G. Boos[23], A. Dossanov[23], N.S. Pokrovskiy[23], B.O. Zhautykov[23], D. Son[24], J. de Favereau[25], K. Piotrzkowski[25], F. Barreiro[26], C. Glasman[26,m], M. Jimenez[26], L. Labarga[26], J. del Peso[26], E. Ron[26], J. Terrón[26], M. Zambrana[26], F. Corriveau[27], C. Liu[27], R. Walsh[27], C. Zhou[27], T. Tsurugai[28], A. Antonov[29], B.A. Dolgoshein[29], I. Rubinsky[29], V. Sosnovtsev[29], A. Stifutkin[29], S. Suchkov[29], R.K. Dementiev[30], P.F. Ermolov[30], L.K. Gladilin[30], I.I. Katkov[30], L.A. Khein[30], I.A. Korzhavina[30], V.A. Kuzmin[30], B.B. Levchenko[30,n], O.Y. Lukina[30], A.S. Proskuryakov[30], L.M. Shcheglova[30], D.S. Zotkin[30], S.A. Zotkin[30], I. Abt[31], C. Büttner[31], A. Caldwell[31], D. Kollar[31], W.B. Schmidke[31], J. Sutiak[31], G. Grigorescu[32], A. Keramidas[32], E. Koffeman[32], P. Kooijman[32], A. Pellegrino[32], H. Tiecke[32], M. Vázquez[32,61], L. Wiggers[32], N. Brümmer[33], B. Bylsma[33], L.S. Durkin[33], A. Lee[33], T.Y. Ling[33], P.D. Allfrey[34], M.A. Bell[34], A.M. Cooper-Sarkar[34], A. Cottrell[34], R.C.E. Devenish[34], B. Foster[34], K. Korcsak-Gorzo[34], S. Patel[34], V. Roberfroid[34,o], A. Robertson[34], P.B. Straub[34], C. Uribe-Estrada[34], R. Walczak[34], P. Bellan[35], A. Bertolin[35], R. Brugnera[35], R. Carlin[35], R. Ciesielski[35], F. Dal Corso[35], S. Dusini[35], A. Garfagnini[35], S. Limentani[35], A. Longhin[35], L. Stanco[35], M. Turcato[35], B.Y. Oh[36], A. Raval[36], J. Ukleja[36,p], J.J. Whitmore[36], Y. Iga[37], G. D'Agostini[38], G. Marini[38], A. Nigro[38], J.E. Cole[39], J.C. Hart[39], H. Abramowicz[40,62,q], A. Gabareen[40], R. Ingbir[40], S. Kananov[40], A. Levy[40], M. Kuze[41], R. Hori[42], S. Kagawa[42,r], S. Shimizu[42], T. Tawara[42], R. Hamatsu[43], H. Kaji[43], S. Kitamura[43,63], O. Ota[43], Y.D. Ri[43], M.I. Ferrero[44], V. Monaco[44], R. Sacchi[44], A. Solano[44], M. Arneodo[45], M. Ruspa[45], S. Fourletov[46], J.F. Martin[46], S.K. Boutle[47,66], J.M. Butterworth[47], C. Gwenlan[47,s], T.W. Jones[47], J.H. Loizides[47], M.R. Sutton[47,q], C. Targett-Adams[47], M. Wing[47], B. Brzozowska[48], J. Ciborowski[48,64], G. Grzelak[48], P. Kulinski[48], P. Łużniak[48,65], J. Malka[48,65], R.J. Nowak[48], J.M. Pawlak[48], T. Tymieniecka[48], A. Ukleja[48,t], A.F. Żarnecki[48], M. Adamus[49], P. Plucinski[49,u], Y. Eisenberg[50], I. Giller[50], D. Hochman[50], U. Karshon[50], M. Rosin[50], E. Brownson[51], T. Danielson[51], A. Everett[51], D. Kçira[51], D.D. Reeder[51], P. Ryan[51], A.A. Savin[51], W.H. Smith[51], H. Wolfe[51], S. Bhadra[52], C.D. Catterall[52], Y. Cui[52], G. Hartner[52], S. Menary[52], U. Noor[52], M. Soares[52], J. Standage[52], J. Whyte[52]

[1] Argonne National Laboratory, Argonne, Illinois 60439-4815, USA[v]
[2] Andrews University, Berrien Springs, Michigan 49104-0380, USA
[3] Institut für Physik der Humboldt-Universität zu Berlin, Berlin, Germany
[4] University and INFN Bologna, Bologna, Italy[w]
[5] Physikalisches Institut der Universität Bonn, Bonn, Germany[x]

[6] H.H. Wills Physics Laboratory, University of Bristol, Bristol, UK[y]
[7] Calabria University, Physics Department and INFN, Cosenza, Italy[w]
[8] Chonnam National University, Kwangju, South Korea[z]
[9] Jabatan Fizik, Universiti Malaya, 50603 Kuala Lumpur, Malaysia[aa]
[10] Nevis Laboratories, Columbia University, Irvington on Hudson, New York 10027, USA[ab]
[11] The Henryk Niewodniczanski Institute of Nuclear Physics, Polish Academy of Sciences, Cracow, Poland[ac]
[12] Faculty of Physics and Applied Computer Science, AGH-University of Science and Technology, Cracow, Poland[ad]
[13] Department of Physics, Jagellonian University, Cracow, Poland
[14] Deutsches Elektronen-Synchrotron DESY, Hamburg, Germany
[15] Deutsches Elektronen-Synchrotron DESY, Zeuthen, Germany
[16] University and INFN, Florence, Italy[w]
[17] Fakultät für Physik der Universität Freiburg i. Br., Freiburg i. Br., Germany[x]
[18] Department of Physics and Astronomy, University of Glasgow, Glasgow, UK[y]
[19] Department of Engineering in Management and Finance, Univ. of Aegean, Greece
[20] Hamburg University, Institute of Exp. Physics, Hamburg, Germany[x]
[21] Imperial College London, High Energy Nuclear Physics Group, London, UK[y]
[22] Institute of Particle and Nuclear Studies, KEK, Tsukuba, Japan[al]
[23] Institute of Physics and Technology of Ministry of Education and Science of Kazakhstan, Almaty, Kazakhstan
[24] Kyungpook National University, Center for High Energy Physics, Daegu, South Korea[z]
[25] Institut de Physique Nucléaire, Université Catholique de Louvain, Louvain-la-Neuve, Belgium[ae]
[26] Departamento de Física Teórica, Universidad Autónoma de Madrid, Madrid, Spain[af]
[27] Department of Physics, McGill University, Montréal, Québec, Canada H3A 2T8[ag]
[28] Meiji Gakuin University, Faculty of General Education, Yokohama, Japan[al]
[29] Moscow Engineering Physics Institute, Moscow, Russia[ah]
[30] Moscow State University, Institute of Nuclear Physics, Moscow, Russia[ai]
[31] Max-Planck-Institut für Physik, München, Germany
[32] NIKHEF and University of Amsterdam, Amsterdam, Netherlands[aj]
[33] Physics Department, Ohio State University, Columbus, Ohio 43210, USA[v]
[34] Department of Physics, University of Oxford, Oxford, UK[y]
[35] Dipartimento di Fisica dell' Università and INFN, Padova, Italy[w]
[36] Department of Physics, Pennsylvania State University, University Park, Pennsylvania 16802, USA[ab]
[37] Polytechnic University, Sagamihara, Japan[al]
[38] Dipartimento di Fisica, Università 'La Sapienza' and INFN, Rome, Italy[w]
[39] Rutherford Appleton Laboratory, Chilton, Didcot, Oxon, UK[y]
[40] Raymond and Beverly Sackler Faculty of Exact Sciences, School of Physics, Tel-Aviv University, Tel-Aviv, Israel[ak]
[41] Department of Physics, Tokyo Institute of Technology, Tokyo, Japan[al]
[42] Department of Physics, University of Tokyo, Tokyo, Japan[al]
[43] Tokyo Metropolitan University, Department of Physics, Tokyo, Japan[al]
[44] Università di Torino and INFN, Torino, Italy[w]
[45] Università del Piemonte Orientale, Novara, and INFN, Torino, Italy[w]
[46] Department of Physics, University of Toronto, Toronto, Ontario, Canada M5S 1A7[ag]
[47] Physics and Astronomy Department, University College London, London, UK[y]
[48] Warsaw University, Institute of Experimental Physics, Warsaw, Poland
[49] Institute for Nuclear Studies, Warsaw, Poland
[50] Department of Particle Physics, Weizmann Institute, Rehovot, Israel[am]
[51] Department of Physics, University of Wisconsin, Madison, Wisconsin 53706, USA[v]
[52] Department of Physics, York University, Ontario, Canada M3J 1P3[ag]
[53] also affiliated with University College London, UK
[54] also at University of Hamburg, Germany
[55] now at Univ. of Wuppertal, Germany
[56] now at DESY group FEB, Hamburg, Germany
[57] also at Institut of Theoretical and Experimental Physics, Moscow, Russia
[58] also at INP, Cracow, Poland
[59] now at ICEPP, University of Tokyo, Japan
[60] also at University of Tokyo, Japan
[61] now at CERN, Geneva, Switzerland
[62] also at Max Planck Institute, Munich, Germany
[63] Department of Radiological Science, Tokyo Institute of Technology, Tokyo, Japan
[64] also at Łódź University, Poland
[65] Łódź University, Poland
[66] also affiliated with DESY

Received: 2 November 2006 / Revised version: 22 January 2007 /
Published online: 17 February 2007 –

Abstract. A search for stop production in R-parity-violating supersymmetry has been performed in e^+p interactions with the ZEUS detector at HERA, using an integrated luminosity of $65\,\mathrm{pb}^{-1}$. At HERA, the R-parity-violating coupling λ' allows resonant squark production, $e^+d \to \widetilde{q}$. Since the lowest-mass squark state in most supersymmetry models is the light stop, $\widetilde{t}$, this search concentrated on production of $\widetilde{t}$, followed either by a direct R-parity-violating decay, or by the gauge decay to $b\widetilde{\chi}_1^+$. No evidence for stop production was found and limits were set on λ'_{131} as a function of the stop mass in the framework of the minimal supersymmetric standard model. The results have also been interpreted in terms of constraints on the parameters of the minimal supergravity model.

[a] supported by DESY, Germany
[b] deceased
[c] Alexander von Humboldt Fellow
[d] self-employed
[e] retired
[f] formerly U. Meyer
[g] supported by Chonnam National University in 2005
[h] supported by a scholarship of the World Laboratory Björn Wiik Research Project
[i] supported by the research grant no. 1 P03B 04529 (2005-2008)
[j] on leave of absence from FPACS, AGH-UST, Cracow, Poland
[k] e-mail: gallo@mail.desy.de
[l] partly supported by Moscow State University, Russia
[m] Ramón y Cajal Fellow
[n] partly supported by Russian Foundation for Basic Research grant no. 05-02-39028-NSFC-a
[o] EU Marie Curie Fellow
[p] partially supported by Warsaw University, Poland
[q] Alexander von Humboldt Research Award supported by DESY, Germany
[r] now at KEK, Tsukuba, Japan
[s] PPARC Advanced fellow
[t] supported by the Polish Ministry for Education and Science grant no. 1 P03B 12629
[u] supported by the Polish Ministry for Education and Science grant no. 1 P03B 14129
[v] supported by the US Department of Energy
[w] supported by the Italian National Institute for Nuclear Physics (INFN)
[x] supported by the German Federal Ministry for Education and Research (BMBF), under contract numbers HZ1GUA 2, HZ1GUB 0, HZ1PDA 5, HZ1VFA 5
[y] supported by the Particle Physics and Astronomy Research Council, UK
[z] supported by the Korean Ministry of Education and Korea Science and Engineering Foundation
[aa] supported by the Malaysian Ministry of Science, Technology and Innovation/Akademi Sains Malaysia grant SAGA 66-02-03-0048
[ab] supported by the US National Science Foundation
[ac] supported by the Polish State Committee for Scientific Research, grant no. 620/E-77/SPB/DESY/P-03/DZ 117/2003-2005 and grant no. 1P03B07427/2004-2006
[ad] supported by the Polish Ministry of Scientific Research and Information Technology, grant no. 112/E-356/SPUB/DESY/P-03/DZ 116/2003-2005 and 1 P03B 065 27

1 Introduction

Many extensions of the standard model (SM) require a new fundamental symmetry between bosons and fermions, known as *supersymmetry* (SUSY) [1–4]. This symmetry, hypothesizing the existence of supersymmetric partners of the SM particles, with similar properties but with spin changed by one half, controls the divergent higher-order loop corrections to the Higgs-boson mass. Despite numerous searches for such new particles, no evidence has been observed, indicating that supersymmetry, if it exists, becomes manifest at scales beyond the present experimental limit. Since SUSY involves so many parameters, different experimental techniques complement each other.

One important quantum number in supersymmetry models is R-parity (R_p). Its conservation ensures the conservation of both lepton and baryon number. Most of the searches performed at colliders drew conclusions under the assumption of R_p conservation. Nevertheless, the most general supersymmetric extension of the SM Lagrangian contains terms which violate R_p and some of the possible R_p-violating ($\not{R}_\mathrm{p}$) scenarios are compatible with the present experimental constraints.

[ae] supported by FNRS and its associated funds (IISN and FRIA) and by an Inter-University Attraction Poles Programme subsidised by the Belgian Federal Science Policy Office
[af] supported by the Spanish Ministry of Education and Science through funds provided by CICYT
[ag] supported by the Natural Sciences and Engineering Research Council of Canada (NSERC)
[ah] partially supported by the German Federal Ministry for Education and Research (BMBF)
[ai] supported by RF Presidential grant N 1685.2003.2 for the leading scientific schools and by the Russian Ministry of Education and Science through its grant for Scientific Research on High Energy Physics
[aj] supported by the Netherlands Foundation for Research on Matter (FOM)
[ak] supported by the German-Israeli Foundation and the Israel Science Foundation
[al] supported by the Japanese Ministry of Education, Culture, Sports, Science and Technology (MEXT) and its grants for Scientific Research
[am] supported in part by the MINERVA Gesellschaft für Forschung GmbH, the Israel Science Foundation (grant no. 293/02-11.2) and the U.S.-Israel Binational Science Foundation

One of the most interesting consequences of $\not{R}_{\rm p}$ scenarios is the possibility of producing single SUSY particles (sparticles) at colliders. Electron-proton collisions at HERA are well suited to the search for squarks, the scalar supersymmetric partners of quarks, since such states can be produced by an appropriate coupling of the incoming lepton and a quark in the proton.

In most of the SUSY scenarios, the squarks of the third generation are the lightest; the present analysis is aimed of searching for the stop, $\tilde{t}$, the supersymmetric partner of the top quark. At HERA, the stop can be produced resonantly via $e^+d \to \tilde{t}$, up to the ep centre-of-mass energy $\sqrt{s} \simeq 320$ GeV. The stop decay can lead to distinctive topologies with a high-energy positron or neutrino and hadronic jets, which can be efficiently separated from the SM background.

Direct searches for stop production have been already performed at HERA [5, 6], LEP [7–9] and Tevatron [10].

2 Stop phenomenology

The R-parity, defined as $R_{\rm p} = (-1)^{3B+L+2S}$, is a multiplicative quantum number which is 1 for particles and -1 for sparticles (B, L and S denote baryon number, lepton number and spin, respectively). R-parity conservation would imply that supersymmetric particles are always pair produced and the lightest supersymmetric particle (LSP) is stable, a good candidate for cold dark matter.

If R-parity is violated, it is possible to create single sparticles that decay to SM particles [11]. The $\not{R}_{\rm p}$ terms in the SUSY superpotential are given by:

$$W_{\not{R}_{\rm p}} = \lambda_{ijk} L_i L_j \overline{E}_k + \lambda'_{ijk} L_i Q_j \overline{D}_k + \lambda''_{ijk} U_i \overline{D}_j \overline{D}_k \,, \quad (1)$$

where the subscripts i,j,k are the generation indices, L_i denotes the $SU(2)$ doublet lepton superfield, E_i the $SU(2)$ singlet lepton superfield, Q_i the $SU(2)$ doublet quark superfield and D_i and U_i the $SU(2)$ singlet down- and up-type quark superfields. The dimensionless Yukawa couplings λ_{ijk}, λ'_{ijk}, λ''_{ijk} are free parameters of the model.

In the case of stop production in ep collisions, the only terms involved are those parameterized by the Yukawa coupling λ'_{131}. The partners of the left- and right-handed top, $\widetilde{t}_{\rm L}$ and $\widetilde{t}_{\rm R}$, can mix together in two mass eigenstates, $\widetilde{t}_1$ and $\widetilde{t}_2$, which, because of the large top mass, are usually strongly non-degenerate. Due to the chiral properties of the SUSY superpotential (1) only the $\widetilde{t}_{\rm L}$ state contributes to the stop production cross section. In the regime of narrow-width approximation (NWA), the production cross section for the lighter state $\widetilde{t}_1$ is hence:

$$\sigma(e^+p \to \widetilde{t}_1) = \frac{\pi}{4s} \, (\cos\theta_{\widetilde{t}} \cdot \lambda'_{131})^2 \, d(M^2_{\widetilde{t}_1}/s, M^2_{\widetilde{t}_1}) \,, \quad (2)$$

where $d(x, Q^2)$[1] is the parton density of the d quark in the proton and $\theta_{\widetilde{t}}$ is the mixing angle between $\widetilde{t}_1$ and $\widetilde{t}_2$. In this paper only the lighter stop, $\widetilde{t}_1$, denoted hereafter as $\widetilde{t}$, has been considered since contributions from $\widetilde{t}_2$ are negligible for all the considered scenarios. The effects of the initial state photon radiation decreases the stop production cross section of $\sim 5\%$ (20%) for a stop mass of 150(280) GeV and have been taken into account using the Weiszäcker–Williams approach [12, 13]. The NLO QCD corrections have been also included [14], they increase the LO cross section of $\sim 20\%$–25%.

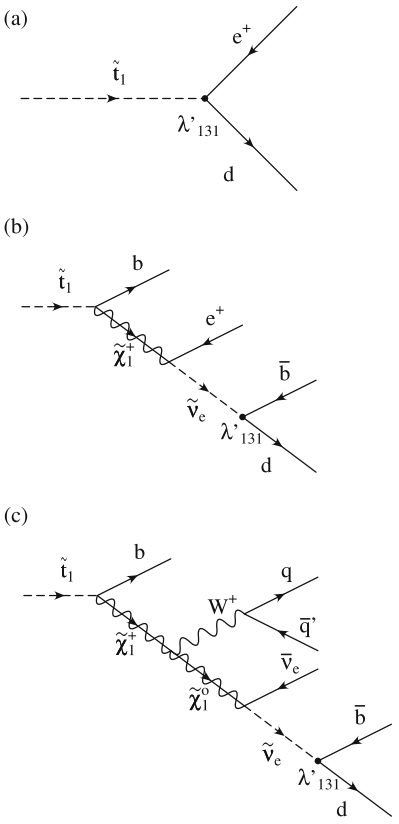

Fig. 1. Considered decay modes of the stop squark: the e-J channel (**a**), the e-MJ channel (**b**) and the ν-MJ channel (**c**)

The $\widetilde{t}$ decays considered in this study are the $R_{\rm p}$-violating channel $\widetilde{t} \to e^+d$ and the $R_{\rm p}$-conserving decay $\widetilde{t} \to \widetilde{\chi}^+_1 b$, where $\widetilde{\chi}^+_1$ is the lightest chargino[2]. These two channels provide a sufficiently large total branching ratio over all of the considered SUSY parameter space. The channel $\widetilde{t} \to \widetilde{\chi}^0_1 t$, where $\widetilde{\chi}^0_1$ is the lightest neutralino[3], contributes only at the highest stop masses, and even then it is below 10%. Branching ratios involving a heavier chargino or neutralino are small in most of the considered parameter space.

The considered decays, including the cascade from the $\widetilde{\chi}^+_1$, are illustrated in Fig. 1. In the present paper only the hadronic W decays are considered, hence final states involving one positron with one jet (e-J), or more than one jets (e-MJ), and one neutrino and multiple-jets (ν-MJ) are studied.

[1] The variables x, Q^2 and y, which is used later on in the paper, are the three Lorentz-invariant quantities characterizing the DIS processes. Q^2 is the negative of the four-momentum-transfer squared, x the fraction of the proton momentum carried by the struck quark and y the inelasticity.

[2] The superpartners of the charged $SU(2)$ gauge bosons and of the charged Higgs bosons mix together in two mass eigenstates named charginos.

[3] The superpartners of the neutral $SU(2)$ gauge bosons and of the neutral Higgs bosons mix together in four mass eigenstates named neutralinos.

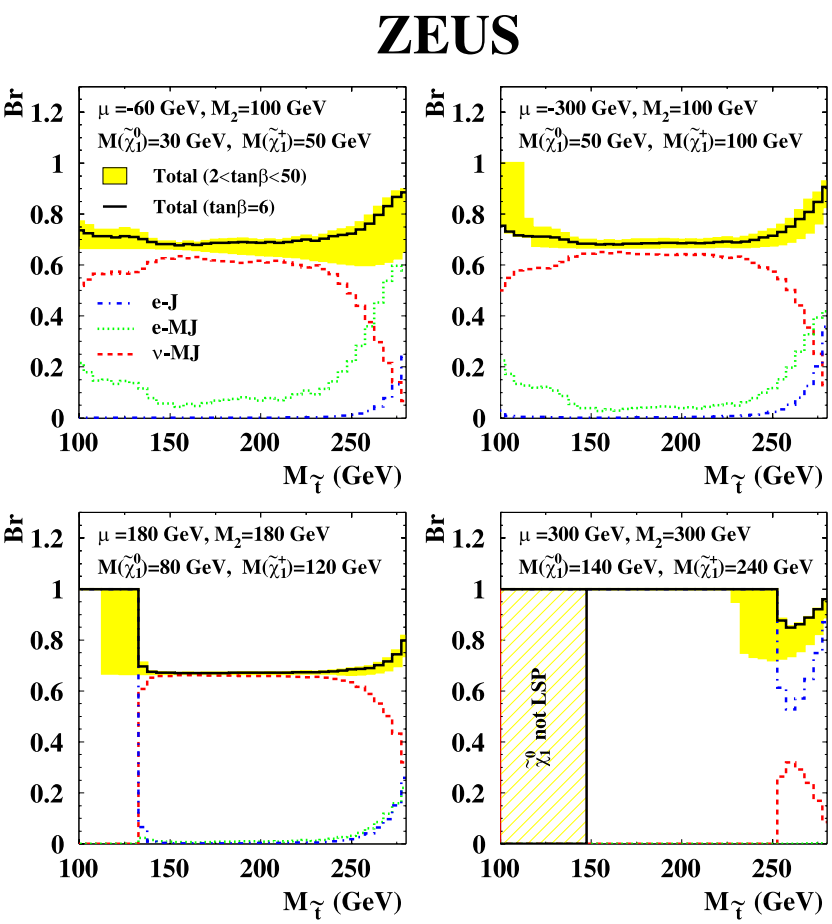

Fig. 2. Branching ratios as a function of the stop mass for different μ and M_2 values, and for λ'_{131} equal to the ZEUS limit for the considered scenarios. The three channels considered in the analysis and their sum are shown for $\tan\beta = 6$. The *shaded band* is the range of the total branching ratio for $2 < \tan\beta < 50$

The results have been interpreted in the context of two different SUSY scenarios: the minimal supersymmetric standard model (MSSM) and the minimal supergravity model (mSUGRA).

In the unconstrained $\not{R}_p$ MSSM [15], the branching ratios for stop decay as well as the masses of the neutralinos, charginos and gluinos[4] are determined by the following MSSM parameters: the mass term μ, which mixes the Higgs superfields; the soft SUSY-breaking parameters M_1, M_2 and M_3 for the $U(1)$, $SU(2)$ and $SU(3)$ gauginos, respectively; $\tan\beta$, the ratio of the vacuum expectation values of the two neutral scalar Higgs fields; and the $\not{R}_p$ Yukawa couplings. The search for the stop was performed in the mass range 100–280 GeV. In order to reduce the number of free parameters, the assumptions listed below were made:

- no mixing between $\widetilde{t}_L$ and $\widetilde{t}_R$ ($\theta_{\widetilde{t}} = 0$);
- only the Yukawa coupling λ'_{131} was assumed to be non-zero;
- SUSY scenarios in which the lightest neutralino $\widetilde{\chi}^0_1$ is not the LSP or is lighter than 30 GeV, already excluded by LEP result [16], were not considered;
- the GUT relations [17, 18] for the gaugino mass terms M_1, M_2 and M_3:

$$M_1 = \frac{5}{3}\tan^2\theta_W \cdot M_2\,,$$

$$M_3 = \frac{\alpha_S}{\alpha_{EM}}\sin^2\theta_W \cdot M_2$$

were assumed. As a consequence, the gluino is always heavier than $\widetilde{t}$, so that the decay $\widetilde{t} \to t\,\widetilde{g}$ is kinematically forbidden;

- all the other sfermions (apart from the lighter stop) were assumed to have large masses that were fixed at 1 TeV.

The total branching ratio due to the considered decay channels is $\gtrsim 70\%$ for the range of parameters $|\mu| < 300$ GeV and M_2 between 100 and 300 GeV that was considered in this analysis.

Figure 2 shows the branching ratios for four representative points in the $\mu - M_2$ plane involving very different masses for $\widetilde{\chi}^0_1$ and $\widetilde{\chi}^+_1$ and for λ'_{131} values equal to the limit given in Sect. 6.2. The shaded band indicates the sum of the three considered channels for $2 < \tan\beta < 50$. The total branching ratio and the contribution of the three channels are shown for the value $\tan\beta = 6$. When the $\widetilde{\chi}^+_1$ mass is larger than the stop mass, the $\not{R}_p$ decay (e-J) is the dominant channel; in the other cases the ν-MJ channel is generally the most relevant.

In the mSUGRA [19–21], the number of free parameters is further reduced by assuming two universal mass parameters at the GUT scale, m_0 and $m_{1/2}$, for all the sfermions and for all the gauginos, respectively. Radiative corrections are assumed to drive the electroweak symme-

[4] Supersymmetric partners of gluons.

try breaking (REWSB), leading to consistency relations that allow the complete model to be fixed, based only on m_0, $m_{1/2}$, the sign of μ, $\tan\beta$, and the common trilinear coupling A_0. In the range of parameters used in this analysis, $m_{1/2} < 180\,\text{GeV}$ and $m_0 < 300\,\text{GeV}$, the total branching ratio of the considered channels is in the range 0.4–0.8 for $m_0 < 200\,\text{GeV}$. For larger values of m_0 it decreases rapidly, since decay channels involving the heavier chargino, which are not considered in this study, become important.

3 Data sample and experimental set-up

The data used in this analysis were collected in the years 1999–2000. The total integrated luminosity was $65.1 \pm 1.5\,\text{pb}^{-1}$ of e^+p collisions. The proton and positron energies were $E_\text{p}^\text{beam} = 920\,\text{GeV}$ and $E_e^\text{beam} = 27.5\,\text{GeV}$, respectively, leading to a centre-of-mass energy of 318 GeV.

A detailed description of the ZEUS detector can be found elsewhere [22]. A brief outline of the components that are most relevant for this analysis is given below.

Charged particles are tracked in the central tracking detector (CTD) [23–25] which operates in a magnetic field of 1.43 T provided by a thin superconducting coil. The CTD consists of 72 cylindrical drift chamber layers, organized in 9 superlayers covering the polar-angle[5] region $15° < \theta < 164°$. The transverse-momentum resolution for full-length tracks is $\sigma(p_\text{T})/p_\text{T} = 0.0058 p_\text{T} \oplus 0.0065 \oplus 0.0014/p_\text{T}$, with p_T in GeV.

The high-resolution uranium–scintillator calorimeter (CAL) [26–29] consists of three parts: the forward (FCAL), the barrel (BCAL) and the rear (RCAL) calorimeters. Each part is subdivided transversely into towers and longitudinally into one electromagnetic section (EMC) and either one (in RCAL) or two (in BCAL and FCAL) hadronic sections (HAC). The smallest subdivision of the calorimeter is called a cell. The CAL energy resolutions, as measured under test-beam conditions, are $\sigma(E)/E = 0.18/\sqrt{E}$ for electrons and $\sigma(E)/E = 0.35/\sqrt{E}$ for hadrons, with E in GeV.

The luminosity was measured using the bremsstrahlung process $ep \to ep\gamma$. The resulting small-angle energetic photons were measured by the luminosity monitor [30–32], a lead-scintillator calorimeter placed in the HERA tunnel at $Z = -107\,\text{m}$.

4 Monte Carlo simulation

The signal processes were simulated with the Monte Carlo (MC) event generator *Susygen* 3 [33]. It uses the exact matrix element for the production and for the decays of sparticles, includes initial- and final-state radiative corrections and is interfaced to *Pythia* 6.2 [34] for the hadronization of the final state. The program *Suspect* 2.1 [35] was used to solve the REWSB consistency relations that determine the sparticle mass spectrum at the electroweak scale in the mSUGRA model.

The dominant background process to the e-J and e-MJ channels is neutral current deep inelastic scattering (NC DIS). For the e-J channel, the background is due to $2 \to 2$ scatters between high-x quarks and the positron. Backgrounds to the e-MJ channel occur in NC DIS events where multi-jet final states result from higher-order QCD effects.

The primary background to the ν-MJ channel comes from charged current deep inelastic scattering (CC DIS) with multiple jets from QCD radiation. An additional background source involves photoproduction events for which the measured transverse momentum is large due to energy mismeasurement.

The NC and CC events were simulated using the *Heracles* 4.6.1 [36] program with the *Djangoh* 1.1 [37] interface to the hadronization program and using the CTEQ5D [38] set of parton distribution functions (PDFs). In *Heracles*, corrections for initial-state and final-state electroweak radiation, vertex and propagator corrections, and two-boson exchange are included. The colour-dipole model of *Ariadne* 4.10 [39] was used to simulate the order α_S plus leading-logarithmic corrections to the quark-parton model. The MEPS model of *Lepto* 6.5 [40] was used as a systematic check. Both programs use the Lund string model of *Jetset* 7.4 [41–43] for the hadronization.

Photoproduction events were simulated using the *Herwig* 6.100 [44] generator, using the CTEQ4L [45] proton PDFs. Both direct and resolved photoproduction were considered. In the direct case, all of the photon energy participates in the hard scattering, whereas, for the resolved process, only a fraction of the photon energy, associated with a parton constituent of the photon, participates in the hard subprocess. For the simulation of the resolved subprocess, the GRV-G [46] photon PDFs were used.

5 Event selection

The signal events are characterized by a high-energy lepton in the final state. In the case of a positron in the final state (e-J and e-MJ channels), the trigger selection was based on a standard neutral current trigger, which required a scattered positron, as used in searches for resonance states decaying to eq [47] and in ZEUS NC DIS studies [48]. For the neutrino case (ν-MJ channel), a trigger selection based on a missing-P_T requirement and already employed in the ZEUS CC DIS analysis [49] was used.

The offline signal-search procedure was performed in two steps [50]. Initially, a preselection was applied to select NC or CC events. Finally, more restrictive selections, optimized to get the best limits in the case of no signal, were applied.

[5] The ZEUS coordinate system is a right-handed Cartesian system, with the Z axis pointing in the proton beam direction, referred to as the "forward direction", and the X axis pointing left towards the centre of HERA. The coordinate origin is at the nominal interaction point.

5.1 Preselection for e^+ final states

The following conditions, some of which were also used at the trigger level with a lower threshold, were designed to select a sample of high-Q^2 NC events:

- Z-coordinate of the event vertex compatible with an ep interaction, $|Z_{\rm vtx}| < 50$ cm;
- a high-energy positron reconstructed from calorimeter and tracking information [51]. A positron energy $E_e > 8$ GeV was required. This cut was increased to $P_{{\rm T},e} > 20$ GeV ($P_{{\rm T},e}$ is the transverse momentum of the positron measured by the calorimeter) for very forward positrons ($\theta_e < 0.3$, where θ_e is the positron polar angle) which are outside the acceptance of the CTD;
- $45 < E - P_{\rm Z} < 70$ GeV, where E and $P_{\rm Z}$ are the total energy and the Z-component of the total momentum of the final state. For NC DIS events, where only particles in the very forward direction escape detection, $E - P_{\rm Z} \sim 2E_e^{\rm beam} = 55$ GeV;
- $Q^2_{\rm DA} > 1000\,{\rm GeV}^2$ and $0.2 < y_{\rm DA} < 0.98$, where $Q^2_{\rm DA}$ and $y_{\rm DA}$ are the DIS kinematic variables reconstructed using the double angle method [52]. The above conditions were imposed in order to restrict the search to a region where the signal is enhanced with respect to NC DIS and the reconstruction of the kinematic variables is reliable;
- $M_{eX} > 100$ GeV, where M_{eX} is the invariant mass of the positron and the hadronic system evaluated using the following relation that exploits the conservation of momentum and $E - P_{\rm Z}$:

$$M^2_{eX} = 2E_e^{\rm beam} \sum_i (E + P_{\rm Z})_i \,. \qquad (3)$$

The sum runs over the final-state positron and all other energy deposits with a polar angle > 0.1, to exclude contributions from the proton remnant.

The bias and resolution of the reconstructed mass were evaluated using the signal MC. On average, the mass was slightly overestimated at low masses (3% at 100 GeV), while the agreement improved towards high masses (< 1% above 150 GeV). The resolution varied between 5% and 1.5% in the mass range 100–280 GeV. After the preselection cuts, 2368 events remained, in good agreement with the expectation of the SM MC of 2430^{+90}_{-252} events, where the error is dominated by the systematic uncertainties described in Sect. 6.1. The SM prediction is dominated by the NC DIS contribution.

Figure 3 shows the distributions of $P_{{\rm T},e}$, $y_{\rm DA}$, $\log_{10}(Q^2_{\rm DA})$ and $P_{\rm T,antipar}/P_{\rm T,par}$ for data and MC; reasonable agreement is seen for all variables. The quantities $P_{\rm T,par}$ and $P_{\rm T,antipar}$ are the parallel and antiparallel components of the hadronic transverse momentum ($P_{\rm T,had}$)

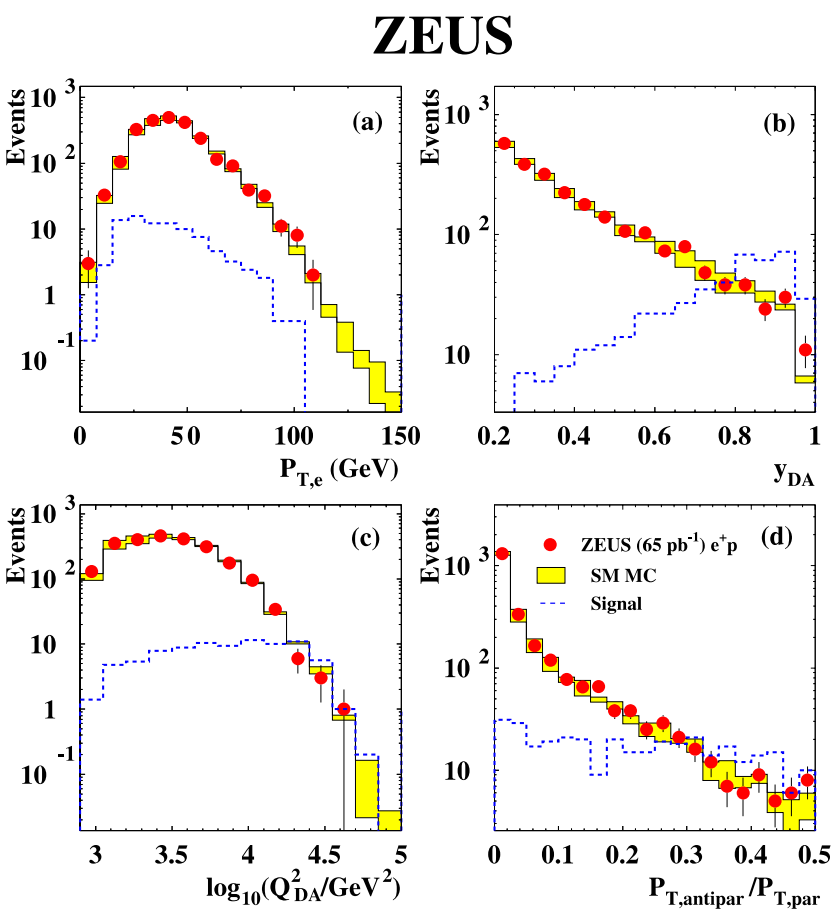

Fig. 3. Comparison between data (*dots*) and SM MC (*histograms*) for (**a**) $P_{{\rm T},e}$, (**b**) $y_{\rm DA}$, (**c**) $\log_{10}(Q^2_{\rm DA})$ and (**d**) $P_{\rm T,antipar}/P_{\rm T,par}$ after the preselection for e^+ final state. The *band* represents the SM expectation with its uncertainty. The MSSM signal for the e-MJ channel (*dashed line*) with $M_{\tilde{t}} = 220$ GeV, $M_2 = 100$ GeV and $\mu = -300$ GeV is also shown, with arbitrary normalization

defined as:

$$P_{\mathrm{T,par}} = \frac{1}{|\mathbf{P}_{\mathrm{T,had}}|} \cdot \sum_{\mathbf{P}_{\mathrm{T},i}\cdot\mathbf{P}_{\mathrm{T,had}}>0} \mathbf{P}_{\mathrm{T},i} \cdot \mathbf{P}_{\mathrm{T,had}} \,,$$

$$P_{\mathrm{T,antipar}} = \frac{1}{|\mathbf{P}_{\mathrm{T,had}}|} \cdot \sum_{\mathbf{P}_{\mathrm{T},i}\cdot\mathbf{P}_{\mathrm{T,had}}<0} \mathbf{P}_{\mathrm{T},i} \cdot \mathbf{P}_{\mathrm{T,had}} \,,$$

where the sums are over calorimeter deposits with polar angle $\theta > 0.1$, excluding the identified positron. The ratio $P_{\mathrm{T,antipar}}/P_{\mathrm{T,par}}$ is used in the final selection to separate one-jet events ($P_{\mathrm{T,antipar}}/P_{\mathrm{T,par}} \sim 0$) from multi-jet events ($P_{\mathrm{T,\ antipar}}/P_{\mathrm{T,par}} > 0$).

5.2 Preselection for ν final state

Events with a neutrino in the final state have a topology similar to CC DIS. The following selection cuts were applied in order to select a sample of high-Q^2 CC events and suppress the non-ep contribution:

- Z-coordinate of the event vertex compatible with an ep interaction, $|Z_{\mathrm{vtx}}| < 50$ cm;
- no reconstructed positron satisfying the same criteria used in e^+ final-state preselection;
- high missing transverse momentum, $P_{\mathrm{T,miss}} > 20$ GeV, where $P_{\mathrm{T,miss}}$ is the missing transverse momentum as measured by the CAL;
- $0.2 < y_{\mathrm{JB}} < 0.95$, where y_{JB} is reconstructed using the Jacquet–Blondel method [53].

The analogue of (3) for the invariant mass of the ν-hadronic system was derived assuming that the missing P_{T} and $E - P_{\mathrm{Z}}$ resulted from a single neutrino:

$$M^2_{\nu X} = 2E_e^{\mathrm{beam}} \left(\sum_i (E + P_{\mathrm{Z}})_i + \frac{P^2_{\mathrm{T,miss}}}{2E_e^{\mathrm{beam}} \cdot (1 - y_{\mathrm{JB}})} \right).$$

The mass resolution varied between 10% and 3% in the mass range 100–280 GeV. On average, the mass was slightly underestimated at high masses (1.5% at 280 GeV), while the agreement improved towards low masses (< 1% above 120 GeV). After the CC preselection cuts 265 events survived, in good agreement with the expectation of the SM MC of 277^{+18}_{-21}. The SM prediction is dominated by CC DIS events, with a small contribution coming from photoproduction processes.

Figure 4 shows the distributions of $P_{\mathrm{T,miss}}$, y_{JB}, $\log_{10}(Q^2_{\mathrm{JB}})$, where the Q^2_{JB} is reconstructed using the Jacquet–Blondel method, and $P_{\mathrm{T,antipar}}/P_{\mathrm{T,par}}$ for data and MC; reasonable agreement is observed for all the variables.

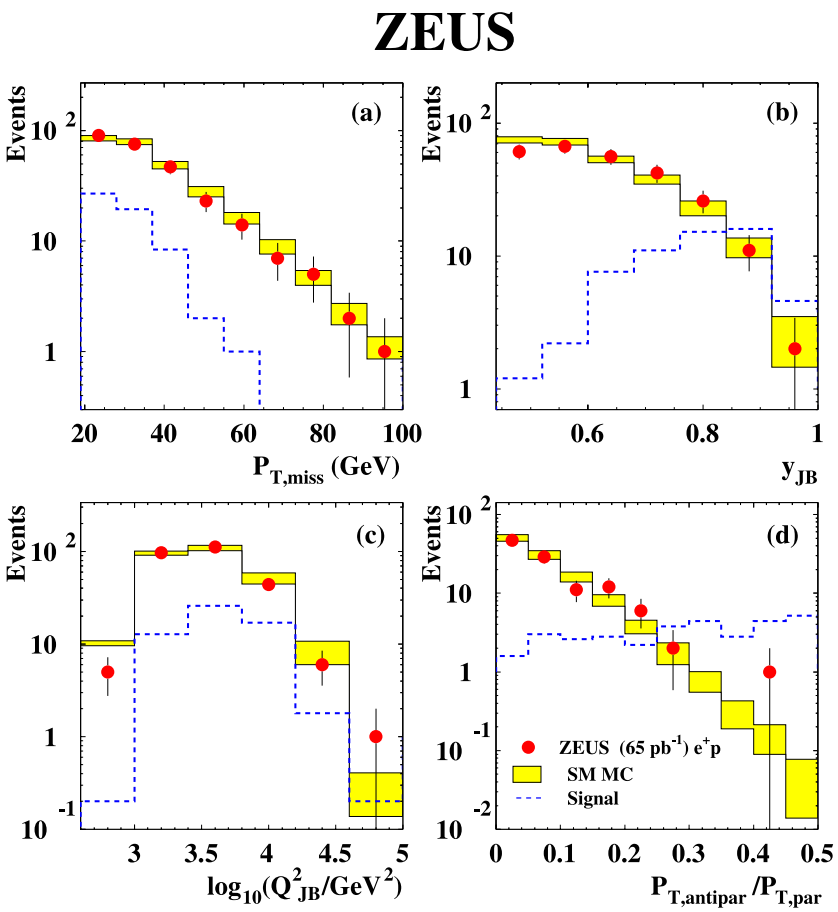

Fig. 4. Comparison between data (*dots*) and SM MC (*histograms*) for (**a**) $P_{\mathrm{T,\ miss}}$, (**b**) y_{JB}, (**c**) $\log_{10}(Q^2_{\mathrm{JB}})$ and (**d**) $P_{t,\ \mathrm{antipar}}/P_{t,\ \mathrm{par}}$ after the preselection for ν final state. The *band* represents the SM expectation with its uncertainty. The MSSM signal (*dashed line*) with $M_{\tilde{t}} = 220$ GeV, $M_2 = 100$ GeV and $\mu = -300$ GeV is also shown, with arbitrary normalization

5.3 Final selection for e^+ final state

The final selection for the channels with a final-state positron was designed to reduce further the contamination from NC DIS by requiring high-Q^2 and high-y events. The following cuts were applied:

- $Q^2_{\rm DA} > 3000\,{\rm GeV}^2$;
- $y_{\rm DA} > y_{\rm cut}$, where $y_{\rm cut}$ was optimized as a function of the reconstructed mass using the SM MC and ranges between 0.7 and 0.4 for masses between 100 and 280 GeV. This cut exploits the different y-dependence of NC DIS, steeply decreasing as y^{-2}, and of a scalar resonance, which has a substantial contribution from large y.

Finally, a cut on $P_{\rm T,antipar}/P_{\rm T,par}$ was used to produce two samples enriched with either one-jet or multi-jet events. The e-J (e-MJ) final sample was defined requiring:

- $P_{t,\rm antipar}/P_{t,\rm par} < (>)\ 0.05$.

Signal efficiencies were evaluated by generating samples of signal events using *Susygen* for different values of the MSSM or mSUGRA parameters. For the e-J channel, the efficiencies ranged between 10 and 45% in the mass range 100–260 GeV, decreasing to 20% at 280 GeV. For the MSSM scenario, the efficiencies for the e-MJ channel were in the range 5%–25% for stop masses between 200 and 280 GeV, depending mainly on the masses of stop and χ_1^+; the efficiency decreased towards lower and higher stop masses. For the mSUGRA scenario, the efficiencies for the e-MJ channel were in the range 5%–15% in most of the parameter space. Table 1 shows good agreement between the number of selected events and SM expectation. Figure 5a

Table 1. Summary of final selection cuts, number of observed and expected events for the SM and signal efficiencies for MSSM ($M_{\tilde{t}} = 220$ GeV) for the different channels discussed in the text

Channel	$Q^2_{\rm DA}$ (GeV^2)	$y_{\rm cut}(M_{\tilde{t}})$	$P_{\rm T,antipar}/P_{\rm T,par}$	Data	SM	Eff. MSSM
e-J	> 3000	0.4–0.7	< 0.05	85	$74.5^{+3.5}_{-6.0}$	0.3
e-MJ	> 3000	0.4–0.7	> 0.05	63	$58.8^{+3.0}_{-5.0}$	0.15–0.2
ν-MJ	–	0.6	> 0.1	19	$20.9^{+1.5}_{-1.6}$	0.15–0.35

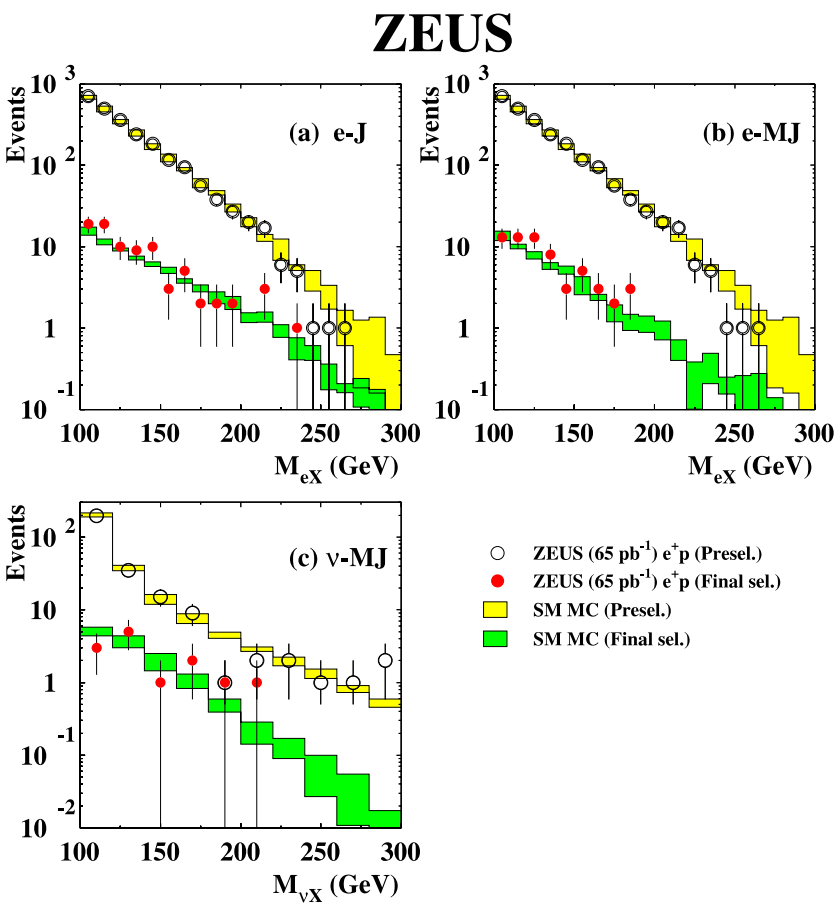

Fig. 5. Reconstructed mass for (**a**) e-J, (**b**) e-MJ and (**c**) ν-MJ channels. The data (*dots*) and SM MC (*histograms*) after preselection (*empty circles* and *light histograms*) and final selection (*filled circles* and *dark histograms*) are shown. The *band* represents the SM expectation with its uncertainty

and b show reconstructed mass distributions of data and SM MC for the e-J and e-MJ preselection and final samples. The data distributions are well described by the SM simulation.

5.4 Final selection for ν final state

In order to enhance stop sensitivity and reduce further the contribution of CC DIS, the final selection required:

- $y_{\rm JB} > 0.6$;
- $P_{t,\rm antipar}/P_{t,\rm par} > 0.1$.

For the MSSM scenario, the efficiencies were in the range 15%–35% for stop masses between 180 and 280 GeV, depending mainly on the masses of the stop and $\widetilde{\chi}_1^0$; the efficiency decreased towards lower and higher stop masses. For the mSUGRA scenario, the efficiencies were in the range 5%–20% in most of the considered parameter space. Table 1 shows good agreement between the number of selected events and the SM expectation.

Figure 5c shows reconstructed mass distributions of data and SM MC for the ν-MJ preselection and final samples. The MC simulation also in this case describes the data reasonably well.

6 Results

Since no evidence for stop production was found, limits at 95% CL were set using a Bayesian approach. The limits were set for two different SUSY scenarios: the unconstrained MSSM model and the mSUGRA model (see Sect. 2).

6.1 Systematic uncertainties

In the calculation of the upper limit on λ'_{131}, several sources of systematic uncertainties were considered. The following systematic uncertainties on the SM background expectation were evaluated:

- the uncertainty from the proton PDFs, evaluated using the procedure suggested by the CTEQ group [54], was $\pm 4\%$ for ν-MJ and $\pm 2\%$ for e-MJ and e-J;
- the uncertainty on the calorimeter energy scale of $\pm 1\%$ ($\pm 2\%$) for the electromagnetic (hadronic) section led to an uncertainty on the SM event rate of $\pm 5\%$ for ν-MJ and $^{+1\%}_{-3\%}$ for e-MJ and e-J;
- the use of MEPS instead of *Ariadne* to simulate the QCD cascade led to an uncertainty of -3% for ν-MJ and -6% for e-MJ and e-J;
- the uncertainty in the integrated luminosity measurement was $\pm 2.25\%$.

In addition, the following uncertainties related to the signal simulation were considered:

- the uncertainties in the signal efficiency due to interpolation between different SUSY scenarios was $\pm 15\%$;
- the theoretical uncertainty on the signal cross section due to the uncertainty in the d-quark parton density [54] in the proton varied from $\pm 3\%$ to $\pm 80\%$ for masses between 100 and 280 GeV.

6.2 Limits for the MSSM model

Assuming the MSSM model, the upper limits on λ'_{131} were evaluated as a function of the stop mass. A scan of the mass spectrum in 1 GeV steps was performed using a sliding window of $\pm 2\sigma_{M_{\widetilde{t}}}$ for $M_{\ell X} < 250\,\text{GeV}$ ($\ell = e$ or ν), where $\sigma_{M_{\widetilde{t}}}$ is the stop mass resolution. For masses larger than 250 GeV, where the SM background is smaller and the expected signal width larger, the condition $M_{\ell X} > M_{\widetilde{t}} - 2\sigma_{M_{\widetilde{t}}}$ was applied.

At each stop mass, the 95% CL limit on λ'_{131} was evaluated using, for each channel, the data events, the SM predictions and the signal expectation for the corresponding mass window. The signal cross section was calculated in the NWA (2), including initial-state radiation for the incoming positron [12, 13] and the next-to-leading-order QCD [14] corrections, using the CTEQ6 [54] set of parton densities, while the branching ratios for the different channels and MSSM scenarios were taken from the *Susygen* simulation. The total likelihood was evaluated as the product of the Poissonian likelihoods of each channel. The systematic uncertainties described in Sect. 6.1 were included in the likelihood function assuming Gaussian probability

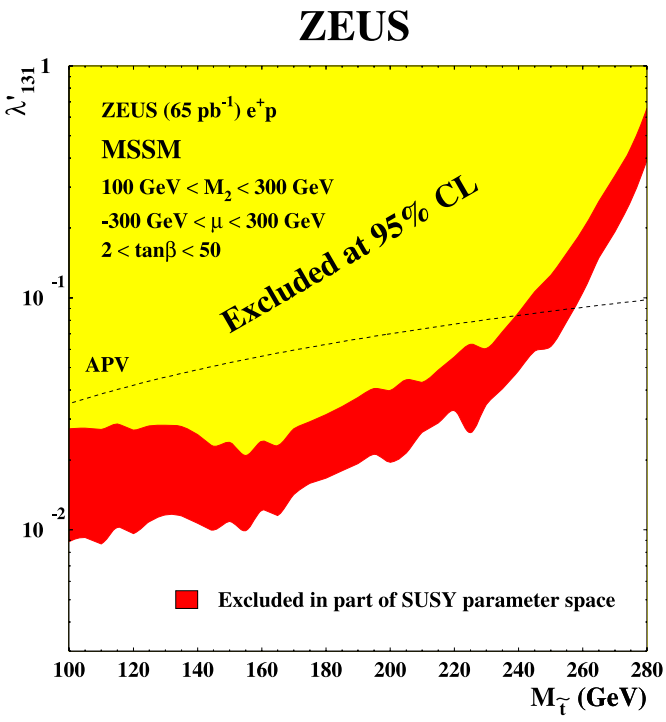

Fig. 6. Exclusion limits on λ'_{131} as a function of the stop mass for the MSSM model. The *light* (*dark*) region is excluded in all (part of) the considered SUSY parameter space. The region above the *dashed line* is excluded by low-energy atomic parity-violation (APV) measurements

densities. A Bayesian approach assuming a flat prior for the signal cross section was then used to produce the limits.

Figure 6 shows the 95% CL limit on λ'_{131} as a function of the stop mass for the range $-300 < \mu < 300$ GeV, $100 < M_2 < 300$ GeV and $2 < \tan\beta < 50$. The limits for masses up to 250 GeV improve on the low-energy constraints from atomic parity-violation (APV) [55] measurements (dashed line) and do not depend strongly on the different SUSY scenarios. The H1 collaboration obtained similar constraints [5, 6] using similar SUSY scenarios.

6.3 Limits for the mSUGRA model

For fixed values of λ'_{131}, constraints on the mSUGRA parameters can be set in the plane (m_0,$m_{1/2}$), when tanβ, A_0 and the sign of μ are fixed. The parameter A_0 enters only marginally at the electroweak scale and was set to zero. Limits at 95% CL were evaluated using a scan of the reconstructed mass spectrum and the same Bayesian approach as in the MSSM case.

Figure 7 shows the 95% CL excluded area in the plane (m_0,$m_{1/2}$) for λ'_{131}=0.3, $\tan\beta = 6$ and $\mu < 0$ (hatched area). The dark region corresponds to values of parameters where no REWSB solution is possible, while the light region corresponds to neutralino masses less than 30 GeV, already excluded by LEP [16]. The dashed lines indicate curves of constant stop mass close to the border of the excluded area. Stop masses can be excluded up to 250 GeV for m_0 smaller than 240 GeV. The effects of the SUSY radiative corrections on the sparticle mass spectrum is included in SUSPECT and have been taken into account. Such effects increase the stop mass and consequently worsen the limits especially at large m_0. For example the point $m_0 = 200$ GeV, $m_{1/2} = 110$ GeV is at the boundary of the ZEUS exclusion region and corresponds to $M_{\tilde{t}} = 256$ GeV. The same point, if SUSY radiative corrections are neglected, corresponds to $M_{\tilde{t}} =$ 243 GeV and would be well inside the ZEUS excluded region.

A scan towards large $\tan\beta$ was performed assuming $M = m_0 = m_{1/2}$. Figure 8 shows the limits on M as a function of $\tan\beta$ for λ'_{131}=0.3 and $\mu < 0$. The limit on M slightly increases from 130 to 140 GeV in the range $6 < \tan\beta < 40$. For larger values, it drops because the large mixing in the $\tilde{\tau}$ sector results in a light $\tilde{\tau}_1$ state into which the $\tilde{t}$ can decay. The efficiency for detecting such decay is low. The effect of the SUSY radiative corrections is to slightly decrease the overall limit and to shift towards larger $\tan\beta$ the point where the stau branching ratio opens up; neglecting radiative corrections the limit drops at $\tan\beta \simeq 37$. The H1 collaboration obtained

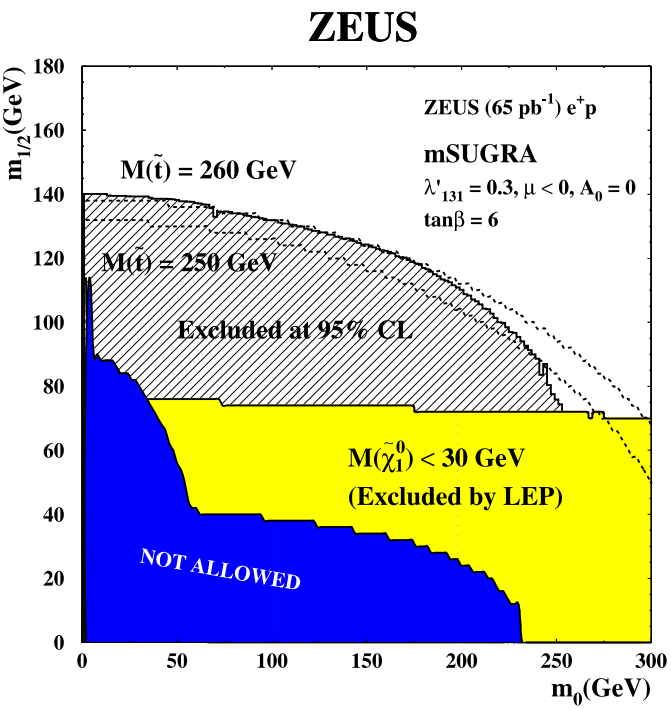

Fig. 7. Exclusion limits for mSUGRA with $\tan\beta = 6$, $\lambda'_{131} =$ 0.3, $\mu < 0$ and $A_0 = 0$ (*hatched area*). The *dark-shaded* region corresponds to values of parameters where no radiative electroweak symmetry-breaking solution is possible. The *light-shaded* region corresponds to neutralino masses (LSP) less than 30 GeV, already excluded by LEP results. The *dashed lines* indicate the curve of constant stop mass close to the border of the excluded region

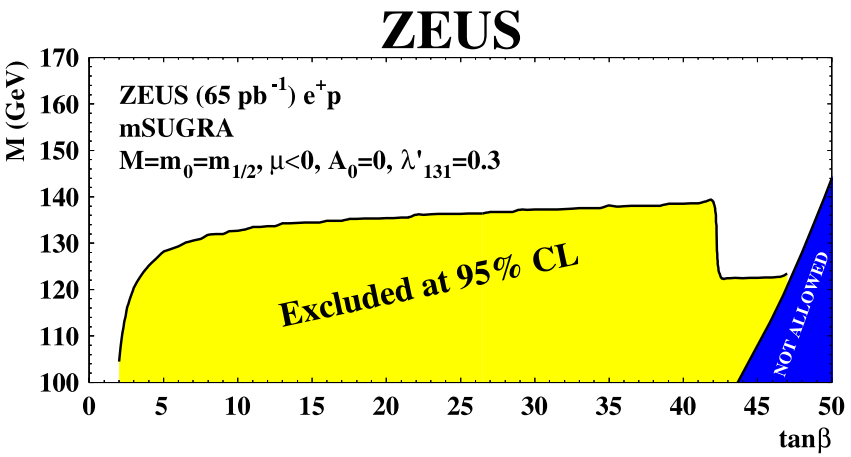

Fig. 8. Exclusion limit for mSUGRA on the mass parameter M ($M = m_0 = m_{1/2}$) as a function of $\tan\beta$ for λ'_{131}=0.3, $\mu < 0$ and $A_0 = 0$. The *dark-shaded* region corresponds to values of parameters where no radiative electroweak symmetry-breaking solution is possible

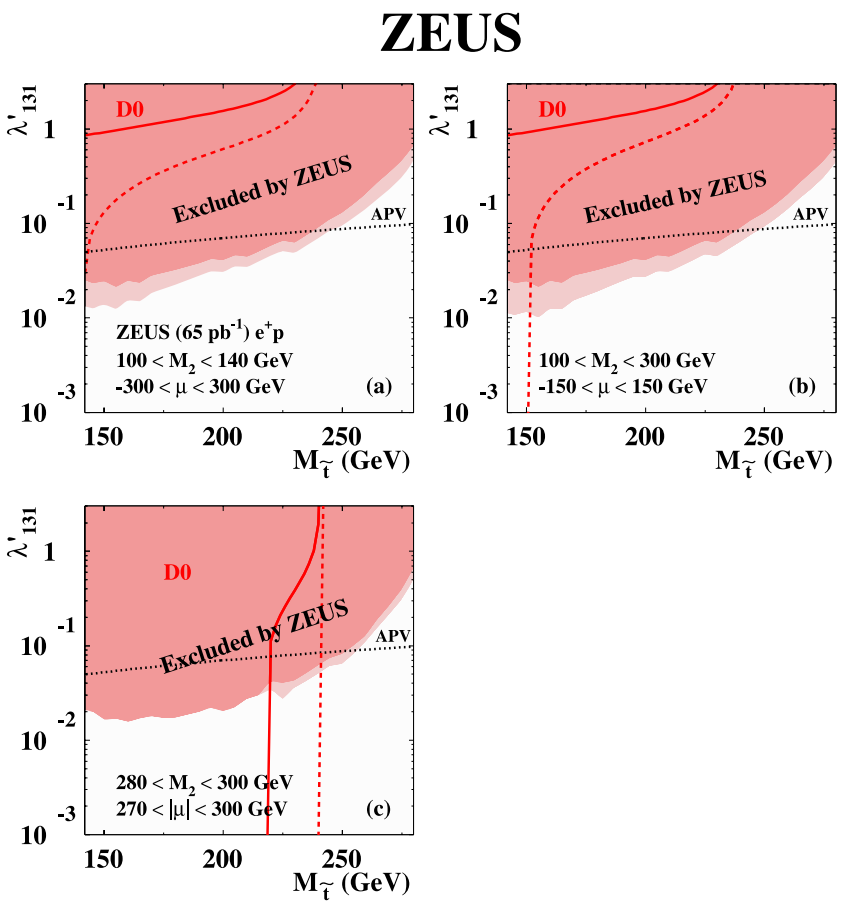

Fig. 9. Comparison between ZEUS, D0 and atomic parity violating (APV) limits in the MSSM scenario for $\tan\beta = 6$ and (**a**) low M_2, (**b**) low $|\mu|$ and (**c**) high M_2 and $|\mu|$. The regions excluded by ZEUS and D0 are shown by the *dark-shaded* area and by the area above the *full line*, respectively. The regions excluded in part of the parameter space are the *light-shaded* area (ZEUS) and the area between the *full* and the *dashed line* (D0). The region of exclusion for atomic parity-violation (APV) is above the *dotted line*

comparable constraints [5, 6] using the same mSUGRA scenarios.

6.4 Comparison to results from other colliders

Studies on stop in $\not{R}_p$ SUSY scenarios have been performed both at LEP [7–9] and the Tevatron [10], looking for the production of stop pairs. LEP mass limits for the stop, in the case of $\lambda' > 0$, were obtained by the OPAL [7] and ALEPH [8] collaborations and are in the range 85–98 GeV. The CDF collaboration [10] set a stop mass limit at 122 GeV assuming $\lambda'_{33k} > 0$ and a branching ratio $B(\widetilde{t} \to b\tau) = 1$.

A more interesting comparison between HERA and Tevatron sensitivities can be done by looking at Tevatron results for leptoquark (LQ) production. The D0 collaboration published limits on leptoquark masses as a function of the branching ratio $B(LQ \to eq)$ [56]. Since leptoquarks and squarks have analogous production mechanisms, such limits can be converted into limits on the stop mass as a function of λ'_{131} [57, 58] and directly compared with the results of this analysis. In the case of the MSSM scenarios, D0 limits are competitive with those of HERA only for the largest values of M_2 and $|\mu|$, where the $\not{R}_p$ decay $\widetilde{t} \to eq$ dominates due to the large chargino mass. For lower values of M_2 or $|\mu|$, the gauge stop decays are relevant and the ZEUS limits improve over those from D0 for masses larger than 150 GeV. Figure 9 shows the comparison between ZEUS and D0 limits for three different regions of the unconstrained MSSM parameter space. In the mSUGRA scenarios considered here, the gauge stop decays are always relevant and thus the ZEUS limits are more stringent than those from D0.

7 Conclusions

A search for stop production in e^+p collisions at HERA was performed using an integrated luminosity of 65 pb^{-1}. No evidence was found for resonances in the decay channels with jet(s) and one high-P_T positron or neutrino. The results have been interpreted in the framework of the R-parity-violating MSSM, setting limits on the Yukawa coupling λ'_{131} as a function of the stop mass. These limits exhibit a weak dependence on the MSSM parameters μ, M_2 and $\tan\beta$ and improve on limits from Tevatron in a large part of the considered parameter space, and on limits from low-energy atomic parity-violation measurements for stop masses lower than 250 GeV. Direct limits on the stop mass have also been derived within the mSUGRA model. In this model only five free parameters determine the full supersymmetric mass spectrum. In this case, for $\lambda'_{131} = 0.3$, $\tan\beta = 6$, $\mu < 0$ and $A_0 = 0$, stop with masses as high as 260 GeV are excluded for a large part of the parameter space.

Acknowledgements. It is a pleasure to thank the DESY Directorate for their strong support and encouragement. The remarkable achievements of the HERA machine group were essential for the successful completion of this work and are greatly appreciated. The design, construction and installation of the ZEUS detector has been made possible by the efforts of many people who are not listed as authors.

References

1. Y.A. Golfand, E.P. Likhttman, JETP Lett. **13**, 323 (1971)
2. D.V. Volkov, V.P. Akulov, JETP Lett. **16**, 438 (1972)
3. D.V. Volkov, V.P. Akulov, Phys. Lett. B **46**, 109 (1973)
4. J. Wess, B. Zumino, Nucl. Phys. B **70**, 39 (1974)
5. H1 Collaboration, A. Aktas et al., Eur. Phys. J. C **36**, 425 (2004)
6. H1 Collaboration, A. Aktas et al., Phys. Lett. B **599**, 159 (2004)
7. OPAL Collaboration, G. Abbiendi et al., Eur. Phys. J. C **33**, 149 (2004)
8. ALEPH Collaboration, A. Heister et al., Eur. Phys. J. C **31**, 1 (2003)
9. L3 Collaboration, P. Achard et al., Phys. Lett. B **524**, 65 (2002)
10. CDF Collaboration, D. Acosta et al., Phys. Rev. Lett. **92**, 051 803 (2004)
11. J. Butterworth, H. Dreiner, Nucl. Phys. B **397**, 3 (1993)
12. C.F. Weizsäcker, Z. Phys. **88**, 612 (1934)
13. E.J. Williams, Phys. Rev. **45**, 729 (1934)
14. T. Plehn et al., Z. Phys. C **74**, 611 (1997)
15. H.K. Dreiner, Perspectives on Supersymmetry, ed. by G.L. Kane (World Scientific, 1997) [hep-ph/9707435]
16. L3 Collaboration, M. Acciarri et al., Eur. Phys. J. C **19**, 397 (2001)
17. H.P. Nilles, Phys. Rep. **110**, 1 (1984)
18. H.E. Haber, G.L. Kane, Phys. Rep. **117**, 75 (1985)
19. R. Barbieri, S. Ferrara, C.A. Savoy, Phys. Lett. B **119**, 343 (1982)
20. L.J. Hall, J. Lykken, S. Weinberg, Phys. Rev. D **27**, 2359 (1983)
21. P. Nath, R. Arnowitt, A.H. Chamseddine, Nucl. Phys. B **227**, 121 (1983)
22. ZEUS Collaboration, U. Holm et al., *The ZEUS Detector* (DESY, 1993), status report (unpublished), available on http://www-zeus.desy.de/bluebook/bluebook.html
23. N. Harnew et al., Nucl. Instrum. Methods A **277**, 176 (1989)
24. B. Foster et al., Nucl. Phys. B Proc. Suppl. **32**, 181 (1993)
25. B. Foster et al., Nucl. Instrum. Methods A **338**, 254 (1994)
26. M. Derrick et al., Nucl. Instrum. Methods A **309**, 77 (1991)
27. A. Andresen et al., Nucl. Instrum. Methods A **309**, 101 (1991)
28. A. Caldwell et al., Nucl. Instrum. Methods A **321**, 356 (1992)
29. A. Bernstein et al., Nucl. Instrum. Methods A **336**, 23 (1993)
30. J. Andruszków et al., Preprint DESY-92-066, DESY, 1992
31. ZEUS Collaboration, M. Derrick et al., Z. Phys. C **63**, 391 (1994)
32. J. Andruszków et al., Acta Phys. Pol. B **32**, 2025 (2001)
33. N. Ghodbane et al., hep-ph/9909499
34. T. Sjöstrand et al., Comput. Phys. Commun. **135**, 238 (2001)
35. A. Djouadi, J. Kneur, G. Moultaka, hep-ph/0211331
36. A. Kwiatkowski, H. Spiesberger, H.J. Mohring, Comput. Phys. Commun. **69**, 155 (1992)
37. K. Charchula, G.A. Schuler , H. Spiesberger, Comput. Phys. Commun. **81**, 381 (1994)
38. CTEQ Collaboration, H.L. Lai et al., Eur. Phys. J. C **12**, 375 (2000)
39. L. Lönnblad, Comput. Phys. Commun. **71**, 15 (1992)
40. G. Ingelman, A. Edin , J. Rathsman, Comput. Phys. Commun. **101**, 108 (1997)
41. T. Sjöstrand, Comput. Phys. Commun. **39**, 347 (1986)
42. T. Sjöstrand, M. Bengtsson, Comput. Phys. Commun. **43**, 367 (1987)
43. T. Sjöstrand, Comput. Phys. Commun. **82**, 74 (1994)
44. G. Marchesini et al., Comput. Phys. Commun. **76**, 465 (1992)
45. CTEQ Collaboration, H.L. Lai et al., Phys. Rev. D **55**, 1280 (1997)
46. M. Gluck et al., Phys. Rev. D **46**, 1973 (1992)
47. ZEUS Collaboration, S. Chekanov et al., Phys. Rev. D **68**, 052 004 (2003)
48. ZEUS Collaboration, S. Chekanov et al., Phys. Rev. D **70**, 052 001 (2004)
49. ZEUS Collaboration, S. Chekanov et al., Eur. Phys. J. C **32**, 16 (2003)
50. A. Montanari, Ph.D. thesis, Alma Mater Università di Bologna, 2001, (unpublished)
51. ZEUS Collaboration, J. Breitweg et al., Z. Phys. C **74**, 207 (1997)
52. S. Bentvelsen, J. Engelen, P. Kooijman, Proc. of the Workshop on Physics at HERA, ed. by W. Buchmüller, G. Ingelman (Hamburg, Germany, DESY 1992), vol 1, p.23
53. F. Jacques, A. Blondel, Proceedings of the Study for an ep Facility for Europe, ed. by U. Amaldi (Hamburg, Germany 1979), p. 391
54. J. Pumplin et al., JHEP **0207**, 012 (2002)
55. P. Langacker, Phys. Lett. B **256**, 277 (1991)
56. D0 Collaboration, V.M. Abazov et al., Phys. Rev. D Rapid Commun. **71**, 071 104(R) (2005)
57. S. Chakrabarti, M. Guchait, N.K. Mondal, Phys. Rev. D **68**, 015 005 (2003)
58. L. Bellagamba, hep-ex/0611012